X-ray scattering study of the interplay between magnetism and structure in CeSb

1997 J. Phys.: Condens. Matter 9 1133

(http://iopscience.iop.org/0953-8984/9/5/017)

J. Phys.: Condens. Matter **9** (1997) 1133–1148. Printed in the UK PII: S0953-8984(97)76749-3

X-ray scattering study of the interplay between magnetism and structure in CeSb

D F McMorrow†, J-G Lussier†, B Lebech†, S Aa Sørensen†, M J Christensen† and O Vogt‡

† Department of Solid State Physics, Risø National Laboratory, DK-4000 Roskilde, Denmark
‡ ETH-Hönggerberg, Laboratorium für Festkorperphysik, CH-8093, Zürich, Switzerland

Received 30 July 1996

Abstract. The chemical and magnetic structures of CeSb have been investigated using high-resolution x-ray scattering techniques. Experiments performed in the non-resonant regime (x-ray energy of $E = 9.4$ keV) showed that when the sample was cooled below its Néel temperature of $T_N \approx 16.5$ K, peaks appeared with commensurate wave vectors $\boldsymbol{q}$. From their polarization and wave-vector dependence, the peaks are deduced to arise mainly from a periodic lattice distortion. In the resonant regime, when the x-ray energy was tuned to the L absorption edges of Ce, weak, resonantly enhanced magnetic scattering was observed at the L_{II} edge ($E = 6.164$ keV), with no scattering found at either L_I or L_{III}. Of the six possible zero-field commensurate magnetic structures reported in earlier neutron experiments, we found the phases with $q_m = \frac{2}{3}$ and $\frac{4}{7}$ only, with the domain that has moments perpendicular to the surface absent. Neutron scattering experiments on the same single crystal confirm that the absence of the other phases is a bulk property of that particular crystal, but the absence of the domain is a feature of the near-surface region. These results are discussed in terms of the currently accepted model of the magnetic structure of CeSb.

1. Introduction

The magnetic phase diagram displayed by CeSb is probably the most complex found among the lanthanide monopnictides, and indeed with at least fourteen distinct phases it is one of the richest of the binary compounds [1]. Although many different techniques have contributed to the unravelling of the full panoply of phases, a detailed understanding of their magnetic structure has relied almost entirely on a series of neutron diffraction studies [2–5]. In contrast to this situation, in the actinide monopnictides much use has been made of recent advances in x-ray scattering techniques. By exploiting the large resonant enhancements to the x-ray magnetic cross-section that exist when the energy is tuned near the atomic M absorption edges of the actinide ion, the magnetism in several members of this series, including UAs [6], NpAs [7, 8], and mixed crystals such as $U_{0.85}Th_{0.15}Sb$ [9], has been studied in some detail. These studies have demonstrated that in certain cases the x-ray is a sensitive probe of both the chemical and magnetic structures and their interaction. For the lanthanides, resonantly enhanced x-ray magnetic scattering has now been observed in most elements of the series at their respective L_{II} and/or L_{III} edges, with Ce being the most notable exception (see, for example, reference [10]). Due to its tendency to form compounds that display various anomalous magnetic properties (heavy fermion, intermediate valence, etc), there is obvious interest in exploring whether x-ray magnetic scattering is a useful probe

0953-8984/97/051133+16$19.50

of the magnetism in this element and its compounds. In this paper we report on an x-ray scattering study of CeSb which reveals the interplay between structure and magnetism in this material.

Table 1. The temperature intervals over which the various commensurate phases are found in CeSb [15]. The errors reflect the widths of the transition region. Because of the small change in wave vector associated with the 4/7, 5/9 and 6/11 phases the transition temperatures were determined around the $3q$-satellite where the peaks from the different phases are resolved.

Magnetic structure $q_m(a^*)$	Lattice distortion $q_l(a^*)$	Temperature range (K)
$\frac{2}{3}$	$\frac{2}{3}$	$16.47 \pm 0.05 \rightarrow 15.97 \pm 0.05$
$\frac{8}{13}$	—	$15.97 \pm 0.05 \rightarrow 15.35 \pm 0.05$
$\frac{4}{7}$	$\frac{2}{7}$	$15.35 \pm 0.05 \rightarrow 13.20 \pm 0.10$
$\frac{5}{9}$	$\frac{2}{9}$	$13.20 \pm 0.10 \rightarrow 10.50 \pm 0.50$
$\frac{6}{11}$	$\frac{2}{11}$	$10.50 \pm 0.50 \rightarrow 8.33 \pm 0.05$
$\frac{1}{2}$	1	$8.33 \pm 0.05 \rightarrow$

CeSb crystallizes in the NaCl-type structure and is a semi-metal. Its magnetic structure has been studied using neutron diffraction by a number of groups over the years, who reach essentially similar conclusions [2–5, 11–13]. (The small differences that have been found are thought to be due to slight variations in sample quality.) Below a Néel temperature of approximately 16.5 K, the Ce^{3+} moments undergo a first-order transition into a longitudinally modulated structure with a commensurable wave vector $\boldsymbol{q}_m = \frac{2}{3}\boldsymbol{a}^*$ ($a = 6.44$ Å), so perpendicular to $\boldsymbol{a}$ the moments couple in ferromagnetic sheets. On further cooling, a series of transitions are made to other commensurable structures, as summarized in table 1. It was soon appreciated that the uniaxial anisotropy holding the Ce ions along the $\langle 100 \rangle$ directions was exceptionally large, and could not be reconciled with the low Néel temperature, or the small crystal-field interaction [14]. A further unusual feature of these structures is that there is a periodic absence of a moment on certain planes, the so-called 'paramagnetic planes' [3], as shown schematically in figure 1; the moments on the other planes carry almost the free-ion value of $gJ \approx 2.14\ \mu_B$.

Various theoretical approaches have been adopted in an attempt to understand the magnetic properties of CeSb. From a purely phenomenological point of view, it has been shown that the general features of the phase diagram of CeSb may be explained by an extended ANNNI model [16]. At a more fundamental level it has been established that the unusual magnetic properties of CeSb arise predominantly from the the proximity of the 4f level to the Fermi energy, giving rise to weak-hybridization effects. Cooper and co-workers have shown that many of the properties of CeSb, including the large uniaxial anisotropy and the excitation spectrum, may be understood on the basis of a phenomenological theory of 'hybridization-mediated' exchange [17, 18]. Beyond these approaches, several groups have performed first-principles electronic structure calculations that have further elucidated the rôle of hybridization [17, 19, 20].

The layout of the paper is as follows. In section 2 we outline the experimental methods used. The results of our non-resonant x-ray scattering experiments are presented in section 3.1.1, and the results of experiments when the energy was tuned to the L edges of Ce are given in section 3.1.2. A brief account of complementary neutron diffraction results from the same crystal as studied with x-rays is then presented in section 3.1.3. In section 4

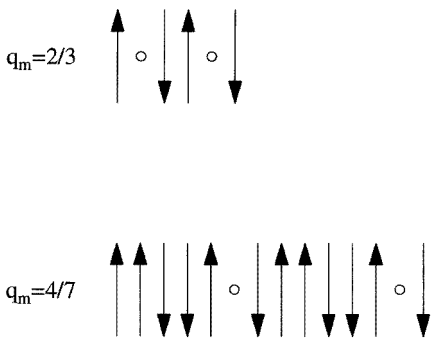

Figure 1. A schematic representation of some of the commensurate spin structures of CeSb found in zero field. For clarity, the phases have been shown with a transverse instead of the longitudinal modulation found in CeSb. Note: the open circles represent the positions of the 'paramagnetic' planes.

our results are discussed with reference to what is known about the magnetic structure of CeSb, and the main points of our work are summarized in section 5. As far as we are aware, there has only been one previous x-ray scattering study of the interplay between structure and magnetism in CeSb: that by Hulliger *et al* [21], who observed a tetragonal distortion of the cubic lattice below T_N.

2. Experimental details

Our first x-ray scattering experiments on CeSb were performed at beamline BW2, Hasylab, and subsequently at beamline X22C, National Synchrotron Light Source (NSLS), Brookhaven National Laboratory. At BW2 a monochromatic beam is produced from the radiation emerging from a 32-pole wiggler by a pair of independent Si(111) crystals, with toroidal mirrors placed either side of the monochromator to focus the beam and to reduce the higher-order contamination. The diffractometer at BW2 operates in the vertical plane, and was equipped with a polarization analyser that allows the detector to either look at the unrotated component of the scattering (the σ–σ channel), or the rotated component (the σ–π channel). The polarization analysis is done in the conventional manner by choosing a material that has a d-spacing such that the Bragg angle is as close to 45° as possible at the particular energy required [22]. The layout of the X22C beamline is somewhat different, in that twin Ge(111) crystals are used to monochromate the radiation from a bending magnet, with just a single mirror upstream of the monochromator. The analyser systems on the two instruments have similar capabilities in principle, although for our experiments we never used the polarization analyser on X22C, opting instead to use a Ge(111) analyser to reduce the background. For the experiments at BW2 a two-stage Displex cryostat, base temperature ≈6.5 K, was used to cool the sample, and was fitted with Be windows. The absorption from the windows was such that we were restricted to working at x-ray energies above about 7 keV. At X22C a three-stage Displex was used, base temperature ≈4 K, and with some of the Be windows replaced by Kapton we were able to work down to the L_{III} edge of Ce ($E = 5.723$ keV), without suffering an appreciable loss of intensity. The same sample and mounting were used at both beamlines. The sample was originally grown by Vogt [23], and is in the form of a cube $5 \times 5 \times 5$ mm^3. The sample was oriented with the (001) zone in the scattering plane as shown in figure 2, with the face normal directions labelled as [h00]. (In

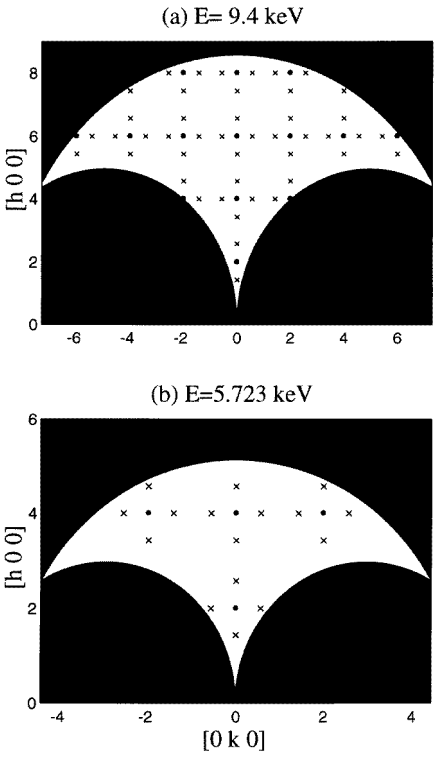

Figure 2. The accessible regions of reciprocal space in the (001) zone at 9.4 keV (top panel) and at the Ce L_{III} edge (5.723 keV) (bottom panel). The filled circles are the allowed charge Bragg peaks, and the crosses mark the positions of the $q_m = \frac{4}{7}$ magnetic peaks assuming that both the (100) and (010) domain are present. A maximum scattering angle of 120° has been assumed.

the same figure the accessible regions of reciprocal space at the two main energies used in our experiments are indicated.) No surface preparation of the crystal was undertaken, and the rocking curve of the (200) Bragg peak was 0.073° (FWHM).

The x-ray magnetic scattering cross-section has been calculated for a longitudinally modulated antiferromagnetic structure, both in the non-resonant [24] and resonant regimes [25]. For simplicity we assume that the incident beam is perfectly linearly polarized in the orbit of the synchrotron, that the modulation is sinusoidal, and that the modulation wave vector, $\boldsymbol{q}$, is parallel to the wave-vector transfer, $\boldsymbol{Q}$, with $\boldsymbol{Q}$ bisecting the incident and scattered beams. In the non-resonant regime the intensity is then non-zero only in the rotated σ–π channel and is given by

$$I(\boldsymbol{Q})_m^{non-res} \propto \sin^6\theta\,|\phi_S|^2\,\delta(\boldsymbol{Q} - \boldsymbol{G} \pm \boldsymbol{q}) \tag{1}$$

where θ is the Bragg angle, ϕ_S is the form factor of the spin moment [24], and $\boldsymbol{G}$ is a reciprocal-lattice vector. Each allowed Bragg peak is thus accompanied by satellite reflections, and in contrast to the neutron magnetic scattering cross-section, the x-ray scattered intensity is sensitive to the component of the moment collinear with $\boldsymbol{Q}$. To obtain an expression for the *resonant* x-ray magnetic cross-section that captures the essential features we proceed with the same assumptions as were made above, and make the additional assumption that the resonant scattering is dominated by dipole E1 processes [26, 27]. This

has been found to be the case in all studies to date, and allows us to write down an expression for the scattered intensity from a longitudinally modulated structure in a particularly simple form, namely

$$I(\boldsymbol{Q})_m^{res} \propto \sin^2\theta\, F^{(1)^2}\, \delta(\boldsymbol{Q} - \boldsymbol{G} \pm \boldsymbol{q}). \tag{2}$$

Here the term $F^{(1)}$ depends on the details of the atomic states between which the resonance occurs, such as the overlap integrals, and lifetimes [27]. As was the case for non-resonant scattering, all of the response is in the rotated σ–π channel. It is worth recalling that a dipole E1 resonance at the L edges of the rare earths involves a 2p–5d transition, and as such the sensitivity to the magnetism comes from the degree to which the 4f moments polarize the 5d bands. (In fact the L_{II} edge is a $2p_{1/2}$–5d transition, while the L_{III} edge is a $2p_{3/2}$–5d one.)

The neutron scattering experiments were performed using the triple-axis spectrometer TAS6, situated on the cold source of reactor DR3, Risø National Laboratory. The spectrometer was operated in an elastic mode with 5 meV neutrons, and collimation selected to give a resolution in the scattering plane of $\approx$0.01 Å^{-1}. Second-order contamination of the beam was suppressed using a Be powder filter. The same sample as was studied by using x-rays was mounted in the (001) zone in a Displex cryostat.

3. Results

3.1. X-ray scattering

3.1.1. The non-resonant regime. We soon established on BW2 that, due to the thick Be vacuum shroud and radiation shields of the cryostat, we would be unable to obtain any useful data around the L absorption edges of Ce. Instead we decided to work at a higher energy of $E = 9.4$ keV, close to the peak in the flux on BW2, and to search for non-resonant magnetic scattering, or for any lattice distortions that may be produced by the magnetic order. For these experiments the instrument was operated in a triple-axis mode with a Ge(111) analyser.

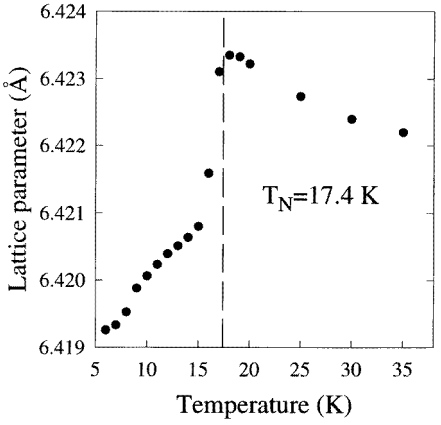

Figure 3. The temperature dependence of the lattice parameter calculated from the position of the (600) Bragg peak. The anomaly near 17 K corresponds to the onset of long-range magnetic order.

It is known that CeSb undergoes a tetragonal distortion due to a magnetoelastic coupling as it is cooled through its Néel temperature of ≈16.5 K [21]. If more than one tetragonal domain forms in the scattering plane, then a splitting of the cubic Bragg peaks will be observed on cooling through T_N. We checked this on our crystal by monitoring the position of the (600) peak as the sample was cooled. The temperature dependence of the lattice parameter is shown in figure 3, where an anomaly is clearly seen at 17.4(2) K. Below this temperature the Bragg peak did not split. In fact no splitting of any of the charge scattering peaks was observed at low temperatures, thus indicating that within the scattering plane there was a single structural domain only.

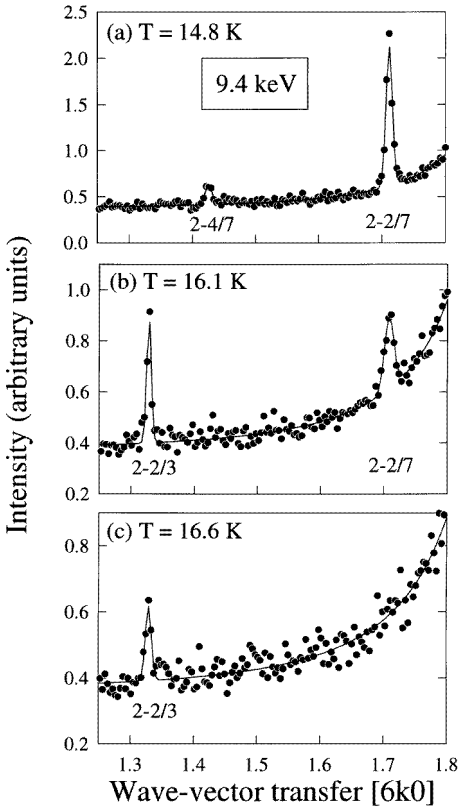

Figure 4. The observed x-ray scattering in scans of the wave-vector transfer along the [6k0] direction at three different temperatures. The x-ray energy was 9.4 keV.

Scans were then performed along the [h00] and [6k0] directions (see figure 2(a)) as the sample was warmed from 5 K. (All of our scans were performed in warming cycles to avoid any problems with hysteresis.) For scans taken up to 10 K no additional satellite peaks were observed. At approximately 10 K a weak satellite peak was found at (6, 1.714, 0), which was indexed as $(6, 2 - \frac{2}{7}, 0)$. On further warming the intensity of this peak increased, and above approximately 12 K an even weaker peak appeared at $(6, 2 - \frac{4}{7}, 0)$ as shown in figure 4(a). For temperatures above 15 K the intensity of both peaks decreased, and a third peak appeared at $(6, 2 - \frac{2}{3}, 0)$, figure 4(b). This peak persisted until just above 17 K, when its intensity decreased rapidly. The data from these scans were analysed by

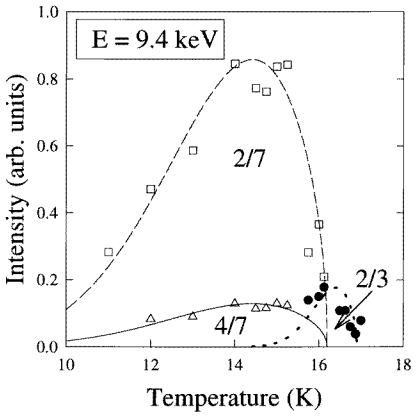

Figure 5. The temperature dependences of the satellite peak intensities at $(6, 2 - \frac{2}{7}, 0)$ and $(6, 2 - \frac{4}{7}, 0)$, observed at an x-ray energy of 9.4 keV. The lines are guides for the eye.

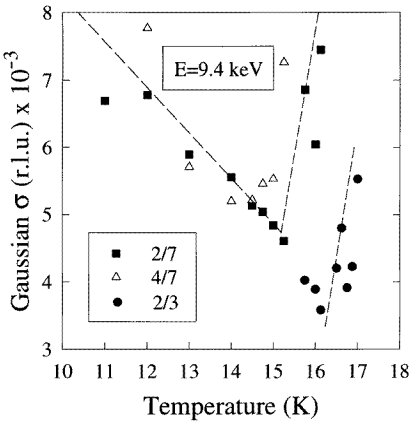

Figure 6. The temperature dependences of the widths of the satellite peaks at $(6, 2 - \frac{2}{7}, 0)$ and $(6, 2 - \frac{4}{7}, 0)$, observed at an x-ray energy of 9.4 keV. The lines are guides for the eye.

fitting the peaks with a Gaussian line shape. The results of this analysis are summarized in figure 5, where the temperature dependences of their intensities are plotted, and in figure 6 where their widths are given.

A wider survey of reciprocal space was then made at 15 K, the temperature at which both the $\frac{2}{7}$ and $\frac{4}{7}$ peaks were most intense. This survey revealed peaks at $(2n, 2m \pm \frac{2}{7}, 0)$ and $(2n, 2m \pm \frac{4}{7}, 0)$, n and m integer, only. Thus these peaks could be associated with a single domain with a propagation wave vector parallel to the surface, because peaks such as $(2n \pm \frac{2}{7}, 2m, 0)$ were absent. This does not, however, prove that the sample is in a single domain, as the third possible [001] axis was perpendicular to the scattering plane. A careful measurement was then made of the integrated intensity of the peaks along the [6k0] direction, within the accessible area shown in figure 2, and in order to establish the $\boldsymbol{Q}$-dependence of the cross-section. The results are shown in figure 7. Instead of attempting to make the usual corrections that have to be applied when comparing the relative intensity of peaks measured at different $\boldsymbol{Q}$s (such as the Lorentz factor and absorption) we fitted the

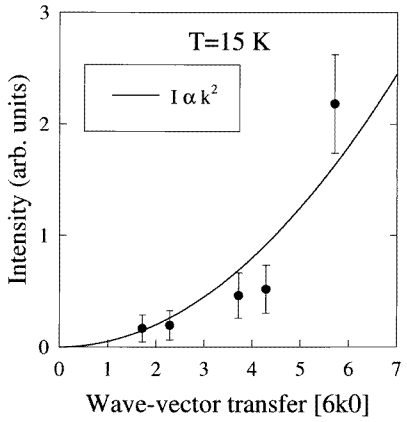

Figure 7. The integrated intensity of the satellite peaks along the [6k0] direction in CeSb at $T = 15$ K, and with $E = 9.4$ keV. The solid line is the result of a best fit to a quadratic variation of the intensity with k, and is discussed in the text.

integrated intensity of the integer-order Bragg peaks along [6k0] to a smooth function. This empirical correction factor was then applied to the satellite intensities. From figure 7 it can be seen that the intensities of the satellite peaks increase approximately quadratically with the component of $\boldsymbol{Q}$ parallel to the surface.

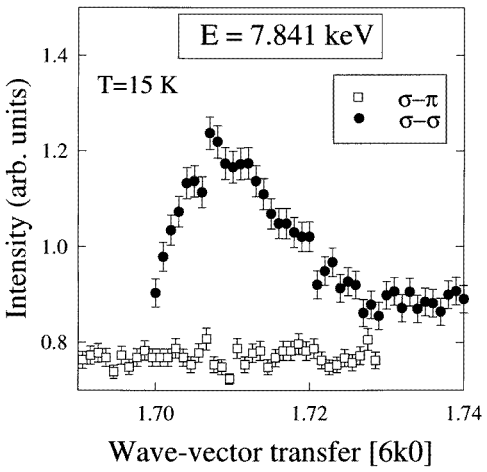

Figure 8. The polarization dependence of the scattering along [6k0] at 15 K and for an x-ray energy of 7.841 keV. The scattering in the σ–π channel has been scaled so that it can be plotted on the same graph as the σ–σ results.

The polarization characteristics of the satellite peaks were then investigated by mounting a pyrolitic graphite (PG) polarization analyser crystal. This crystal was mounted on a turntable which rotates the crystal and detector around the direction of the scattered beam [22]. The energy was tuned to $E = 7.841$ keV, where the Bragg angle of the (006) reflection from PG is exactly 45°, and the sample realigned. The scattering was then measured with the analyser set to monitor the unrotated component of the scattering (the

σ–σ channel), and then the rotated component (the σ–π channel). Away from any atomic absorption edges, the former results from charge scattering, and the latter from magnetic terms in the cross-section. In figure 8 we show the scattering observed in the two channels when the wave-vector was scanned in the vicinity of the $(6, 2-\frac{2}{7}, 0)$ peak. It is clear from this figure that all of the response was in the σ–σ channel. The peaks with wave vectors of $\frac{4}{7}$ and $\frac{2}{3}$ proved to be too weak in intensity to perform this type of polarization analysis on.

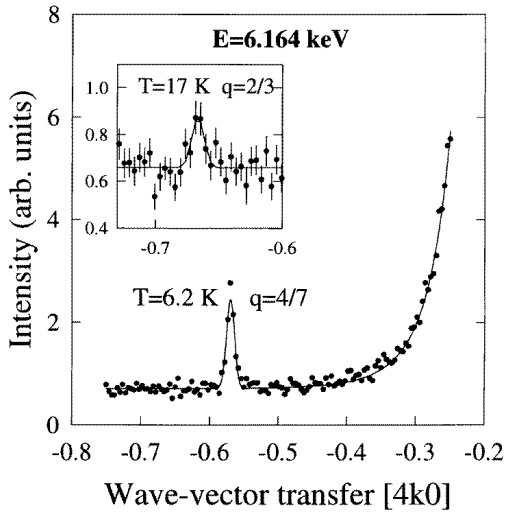

Figure 9. The x-ray scattering along the [4k0] direction in CeSb with the x-ray energy tuned to the L_{II} edge of Ce at 6.164 keV. The main figure shows the data at 6.2 K, where the only satellite peaks observed were at a wave-vector of $q_m = \frac{4}{7}$, and the inset shows the data at 17 K, where a much weaker peak at $q_m = \frac{2}{3}$ was found.

3.1.2. Resonant scattering. The experiments on X22C were mostly performed for x-ray energies around the L edges of Ce, although for comparison with the data from BW2 several scans were also made at 9.4 keV. The energy was first tuned to the Ce L_{II} edge ($E = 6.164$ keV), as it has been reported that, in contrast to the case for the heavy rare earths, the largest enhancements of the magnetic scattering in many of the light rare earths come at L_{II} and not L_{III} [10]. At low temperature, scans along the [4k0] direction revealed the presence of a single satellite peak (and its symmetry-related partners), as shown in figure 9, with a wave vector close to $\frac{4}{7}$. The intensity of this peak decreased smoothly for temperatures above 10 K, while at 17 K a much weaker peak with a wave vector of $\frac{2}{3}$ was observed (see the inset in figure 9). The temperature dependence of the intensity and width of the $\frac{4}{7}$ peak, derived from fitting a Gaussian line shape to the data, are shown in figure 10.

To determine whether or not the $\frac{4}{7}$ peak found at low temperatures arose from a resonant process, and hence was magnetic in origin, the energy dependence of this peak was carefully measured. This was achieved by stepping the energy through the L_{II} edge, and at each energy the crystal rotation angle ϕ was scanned. This allowed us to obtain the integrated intensity as a function of energy, and to correct for the increase in the background from fluorescence above the edge. The results of these scans are summarized in figure 11, where the satellite peak is shown to display a sharp resonance in energy with a width of 7.5(1.0) eV. At resonance the peak count rate was $\approx$40 counts s^{-1} on a background of $\approx$16 counts s^{-1}. For

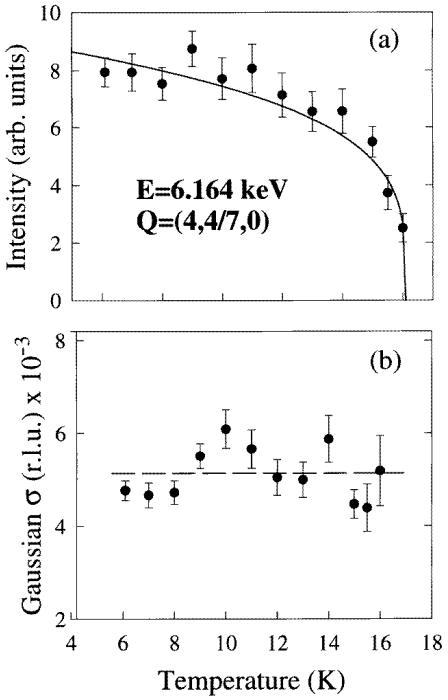

Figure 10. The temperature dependence of (a) the integrated intensity and (b) the width of the $(4, \frac{4}{7}, 0)$ peak as determined by x-ray scattering. The lines are guides for the eye.

comparison the change in intensity of the (400) Bragg peak is shown in the same figure. An exhaustive search was made for any satellite peaks with the x-ray energy tuned to either the L_I or L_{III} edges, without success.

The scans performed at 9.4 keV on X22C were in broad agreement with the results at the same energy from BW2 (see section 3.1.1), in that the dominant phase below T_N had a peak at $\frac{2}{7}$. The main difference was that the peaks were somewhat weaker on X22C owing to the fact that it is more optimized for slightly lower energies. At present we do not know whether we failed to observe the charge satellites in the experiments near the L_{II} edge because the signal-to-noise ratio was insufficient, or because of the difference between the penetration depths λ_d at the two energies used: at 9.4 keV $\lambda_d \approx 50\,000$ Å, whereas at 5.7 keV $\lambda_d \approx 8000$ Å.

3.1.3. Neutron scattering. The motivation for performing a neutron scattering experiment on the same sample as had been studied using x-ray techniques was to allow us to isolate bulk from near-surface properties. With the sample mounted in the (001) zone, scans were performed along the $[2k0]$ and $[hk0]$ directions, for temperatures between 5 and 20 K. At a given temperature, data from these two types of scan were essentially the same, showing that in the bulk the (100) and (010) domains are equally populated, in contrast to the x-ray data where only a single (010) domain was found in the scattering plane. However, the temperature dependences of the wave vectors measured with the two techniques were very similar. At low temperatures the crystal is mostly in the $\frac{4}{7}$ phase (see figure 12(b)), and at higher temperatures the only other phase found was with $q_m = \frac{2}{3}$ (see figure 12(a)).

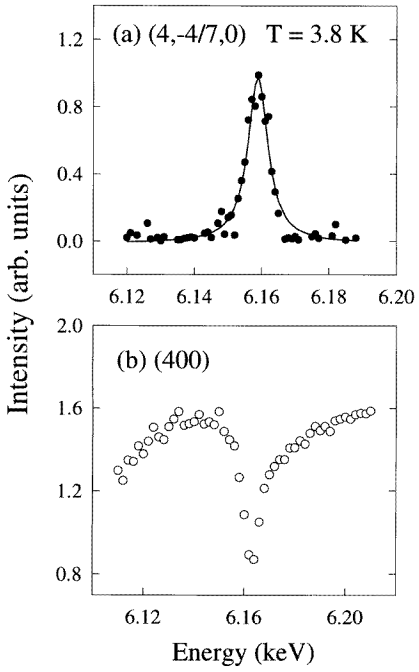

Figure 11. The energy dependence of (a) the $(4, -\frac{4}{7}, 0)$ and (b) the (400) peaks for x-ray energies in the vicinity of the L_{II} edge of Ce. At each point of the resonance curve shown in (b) the integrated intensity was collected by rocking the crystal angle ϕ. The solid line shown in (a) is a Lorentzian with a width of 7 eV (FWHM).

Although our crystal did not display the full range of phases reported for other samples, for a given phase the amplitude of the main magnetic peak relative to that of its satellites was essentially the same as reported earlier [2–5]. We emphasize that all of the satellite peaks observed in the neutron scattering were thus magnetic in origin (see figure 12).

4. Discussion

We will first address the origin of the peaks observed in the non-resonant regime at 9.4 keV. The peaks with wave vectors of $\frac{2}{7}$ and $\frac{4}{7}$ observed at this energy are clearly related, in that they exist in a similar temperature interval (figure 5). We have shown from its polarization characteristics and Q-dependence that the more intense peak with $q = \frac{2}{7}$ arises from charge scattering (figure 8), and that its intensity along the $[6k0]$ direction increases quadratically with k, the component of the wave-vector transfer parallel to the surface (figure 7). The first of these two facts indicates that the peak arises from a modulation of the charge density, with a primary wave vector of $q = \frac{2}{7}$.

In principle the charge density may either be modulated by a periodic displacement of the atoms, or by a modulation of the charge on each fixed lattice site. There is no reason to suppose that the latter occurs in CeSb, while the former may be produced by a magnetoelastic coupling. If we assume that the peak at $\frac{2}{7}$ arises from a sinusoidal distortion, with an amplitude u that is small compared with the lattice spacing a, then the scattered

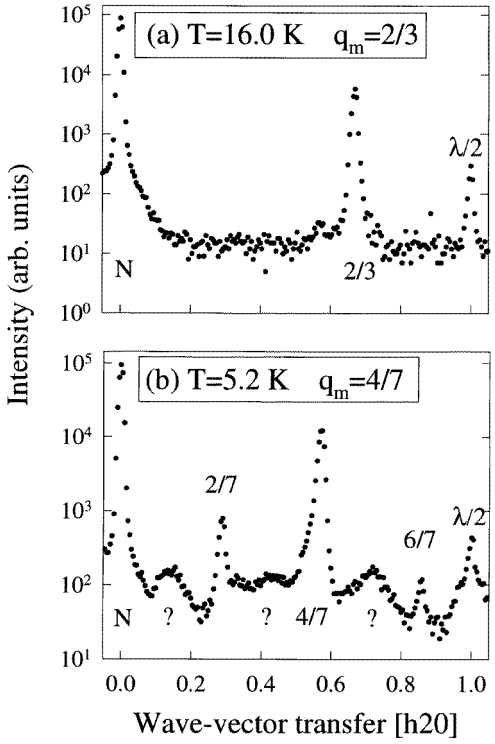

Figure 12. The neutron scattering from CeSb at (a) 16.0 K in the $q_m = \frac{2}{3}$ phase, and (b) at 5.2 K in the $q_m = \frac{4}{7}$ phase. In (a) the peak at $\frac{2}{3}$ is magnetic, while the nuclear peak is at (020). In (b) the main magnetic peak is at $\frac{4}{7}$, with higher-order satellites at $\frac{2}{7}$ and $\frac{6}{7}$. The origin of the broad features in this scan are unknown, but may result from other disordered commensurate phases. The peaks labelled $\lambda/2$ come from second-order contamination of the beam.

intensity may be readily calculated as

$$I(\boldsymbol{Q}) \propto \delta(\boldsymbol{Q}-\boldsymbol{G}) + \left(\frac{\boldsymbol{Q}\cdot\boldsymbol{u}}{2}\right)^2 \delta(\boldsymbol{Q}\pm\boldsymbol{q}-\boldsymbol{G}) + \frac{1}{4}\left(\frac{\boldsymbol{Q}\cdot\boldsymbol{u}}{2}\right)^4 \delta(\boldsymbol{Q}\pm 2\boldsymbol{q}-\boldsymbol{G}). \tag{3}$$

Here $\boldsymbol{q}$ is the wave vector of the distortion, $\boldsymbol{G}$ is a reciprocal-lattice vector, and the calculation has been taken to second order in u/a. Thus it can be seen that even a sinusoidal distortion may produce high-order satellites. The amplitude u may be estimated from the ratio of the intensity of the satellite peak at $(6, 2-\frac{2}{7}, 0)$ to that of the nearest Bragg peak at (620). We have that $I_{2/7}/I_{620} \approx 8.5 \times 10^{-7}$, from which we deduce that $u = 1.0(0.3) \times 10^{-3}$ Å, with the large uncertainty associated with the problem of accurately calibrating the attenuators needed to observe the intense Bragg peaks. (We note that the value of u in CeSb is comparable to that for magnetically induced lattice distortions in other systems, such as Cr for which $u = 4.5 \times 10^{-3}$ Å [28].) It is also clear from equation (3) that the integrated intensity of the $\frac{2}{7}$ peaks should vary as k^2, as shown in figure 7. Equation (3) does not, however, explain the observed relative intensity of the weaker peak at $\frac{4}{7}$. On the basis of this equation the ratio should be $I_{4/7}/I_{2/7} = \frac{1}{16}(Qu)^2 \approx 2.0(0.5) \times 10^{-7}$, whereas it is measured to be $\approx 10^{-1}$.

There are two possible explanations for the origin of the peak at $\frac{4}{7}$. It may either arise

from a lattice distortion with a wavelength half that of the fundamental at $\frac{2}{7}$, or it may arise from non-resonant magnetic scattering. For the former the displacement may again be calculated from equation (3) as $u = 4.5(1.0) \times 10^{-4}$ Å. Whether or not we expect to be able to observe non-resonant magnetic scattering may be determined from the work of Blume [29] who estimated the ratio of magnetic to charge scattering to be

$$\frac{I_{mag}}{I_{charge}} = \left(\frac{\hbar\omega}{mc^2}\right)^2 \left(\frac{f_m}{f}\right)^2 \frac{\langle\mu\rangle^2}{N^2} \tag{4}$$

where $\langle\mu\rangle$ is the average moment, N is number of electrons per atom, f_m and f are the form factors of the magnetic and charge distributions respectively, and the other symbols have their usual meaning. For CeSb we can place an upper estimate of this ratio by putting $\langle\mu\rangle = 2.1\ \mu_B$, the free-ion value for Ce^{3+}, and setting $f_m/f \approx 1$, which gives $I_{mag}/I_{charge} \leqslant 4 \times 10^{-7}$. The effective dynamic range in our experiment on BW2 was $\approx 10^7$ (limited to a large degree by the high background from the sample), so the scattering from the non-resonant magnetic cross-section was close to the limits of observability. We conclude, therefore, that it is possible that the peak at $\frac{4}{7}$ is magnetic in origin, but confirmation of this will require polarization analysis with the subsequent demands of a higher incident flux than was available to us.

The presence of periodic lattice distortions accompanying magnetic order has been observed in several materials. For example, in the incommensurable spin-density-wave phase of Cr there is an associated charge-density wave with a wavelength of one half of the magnetic modulation [28, 30]. A further example, and one that is probably more relevant to the discussion here, is Ho which forms a series of commensurable helical magnetic structures at low temperatures. The existence of these so-called spin-slip phases was first demonstrated using high-resolution x-ray magnetic diffraction by Gibbs *et al* [31]. In addition to the magnetic peaks there were also satellites that arose from charge scattering at distinct commensurable wave vectors. Adopting the notation of Cowley and Bates [32], who performed the first neutron scattering study of the spin-slip phases, the magnetic wave vectors of the spin-slip phases in Ho are given by

$$q_m = q_0\left(\frac{1}{b} + 1\right) \tag{5}$$

where $q_0 = \frac{1}{6}$ is the wave vector of the stable low-temperature phase, and b is the number of atomic planes separating the spin slips. Furthermore, if it is assumed that the lattice is distorted in the region of a slip, through a variation in the magnetoelastic coupling, then the wave vector of the lattice modulation peaks is simply

$$q_l = \frac{2}{b} \tag{6}$$

where the factor of two arises from the two sublattices in the hcp structure of Ho. These simple considerations are in fact capable of explaining the observed positions of the magnetic and lattice modulation peaks in all of the spin-slip phases of Ho. (An equivalent argument to this was given by Gibbs *et al* in their original work [31].)

We can then make a close analogy between Ho and CeSb if we note that for the latter $q_0 = \frac{1}{2}$, and if we identify the 'paramagnetic' plane in CeSb with a spin slip. Thus, most of the commensurable magnetic phases in CeSb may be represented by the series of b-values, namely 3 ($q_m = \frac{2}{3}$), 7 ($q_m = \frac{4}{7}$), 9 ($q_m = \frac{5}{9}$), 11 ($q_m = \frac{6}{11}$) and ∞ ($q_m = \frac{1}{2}$), while the corresponding values of the lattice modulation wave vectors q_l are given in table 1. The missing value in this sequence is $b = 5$, as the phase with $q_m = \frac{3}{5}$ is not observed in CeSb, but instead $q_m = \frac{8}{13}$ between the phases with q_m equal to $\frac{2}{3}$ and $\frac{4}{7}$. The fact that

the $\frac{8}{13}$ phase appears to be different in this sense was also noted in the neutron scattering study by Rossat-Mignod *et al* [3]. From table 1 and these considerations it can be seen that the observed values of $q_l = \frac{2}{3}$ and $\frac{2}{7}$ may be associated with the magnetic phase with $q_m = \frac{2}{3}$ and $\frac{4}{7}$ respectively. (Our neutron scattering study on the same crystal confirmed this assignment, as the temperature ranges over which the two lattice modulation wave vectors were stable were the same as the ranges over which the magnetic wave vectors were observed.) Before going on to consider the results from the resonant regime, we note that our description of the various phases in terms of the parameter b does not have any fundamental significance at this stage, but is more of a convenient way to label the phases so that the wave vectors describing the magnetic order and the lattice distortions may be readily calculated. Moreover, the fact that equations (5) and (6) reproduce the positions of the magnetic and lattice modulation peaks does not actually prove that the 'paramagnetic' planes exist. It is interesting to speculate whether or not a spin-slip model of the magnetic structure in CeSb may be constructed that reproduces the intensities of the observed satellites, without a need to invoke the existence of 'paramagnetic' planes.

We shall now consider briefly the results taken in the resonant regime. One of the most notable aspects of the resonant scattering shown in figure 9 is that at some 40 counts s^{-1} it is extremely weak compared to resonant peaks observed in the other rare earths. For example, we can make a crude comparison with experiments at the L_{II} edge of Pr in random HoPr alloys on the same beamline which gave typical count rates of 1000 counts s^{-1} with a set-up similar to the one that we employed [33], and with experiments on Nd also on the same beamline which gave peak count rates of approximately 3000 counts s^{-1} [10]. (We note that the latter figure quoted was obtained without an analyser crystal, and we expect that the use of an analyser would reduce the intensity by a factor of approximately four.) Unfortunately, because of time constraints we were unable to estimate the absolute value of the enhancement factor at resonance, but the fact that the peaks in CeSb are weak, in the sense described above, is in accordance with an earlier attempt to find the resonant scattering at the L edges of Ce in CeBi which yielded a maximum count rate of 20 counts per minute [34]. A partial explanation for the relative weakness of the Ce resonance is that the relevant parameters (exchange splitting of the 5d band, etc) that determine the amplitude depend on exchange with the 4f electrons, and hence scale with the total spin of the 4f electrons. Thus, if we assume that all other factors are approximately equal, it is expected that the ratio of resonant intensities should scale as the ratio of the square of the total spin moment [35]. For Ce $S = 1/2$, while for Nd $S = 3/2$, from which it can be seen that the difference in spin does not account for the relative weakness of the resonant scattering from Ce, and we conclude that it appears to be anomalously low. (In fact a more refined estimate of the ratio of the resonant scattering from Ce and Nd using the calculations of the Hamrick [35] does not alter this conclusion.) A discussion has recently been given of the variation in the L_{II}-to-L_{III} branching ratio in the rare-earth series by Watson *et al*, and at the present time it is not clear what factors determine the value of this ratio [10].

It is also interesting to compare the temperature dependence of the integrated intensities of the lattice modulation and magnetic peaks shown in figures 5 and 10(a) respectively. From the latter it can be seen that the magnetic intensity rises steeply below 16 K and begins to saturate for temperatures less than 10 K. In contrast the intensity of the lattice modulation peak reaches a maximum at about 15 K, and then on further cooling decreases more slowly, while at the same time the peak broadens (see figure 6). The reason for this behaviour is not known.

Finally, we comment on the fact that the near-surface region has a different domain structure from the bulk, with the domain for moments propagating perpendicular to the

surface absent. The alteration of the domain population in the near-surface region has now been observed in several disparate systems, including Nd [10], Cr [28], and NpAs [7, 8]. In the case of NpAs there is a complex reorientation of the moments with temperature, which is thought to arise from a trade-off between dipole and elastic energies, so at low temperatures the moments point perpendicularly to the surface. For the Cr it was concluded that residual stress in the near-surface region was the decisive factor in selecting a single domain, and we consider that this is the most plausible explanation of the effect in CeSb.

5. Summary

The chemical and magnetic structures of CeSb have been studied in detail using x-ray scattering techniques. Below the Néel temperature, the formation of commensurable magnetic phases produces modulations of the chemical structure. In the near-surface region the domain population of both the chemical and magnetic modulations is different from that of the bulk, with the suppression of the domain that would have the spins perpendicular to the surface. It has been shown how the period of these lattice modulations may be simply related to the period of the magnetic phases. X-ray magnetic resonant scattering has been observed at the L_{II} edge of Ce, and thus the possibility now exists to study more materials containing Ce using this technique.

Acknowledgments

We would like to express our thanks to Roger Cowley and Allan Mackintosh for many illuminating discussions, and to Doon Gibbs for help with the experiments. We are also indebted to the technical staff of Risø, Hasylab, and the NSLS for their support.

References

[1] Vogt O and Mattenberger K 1993 *Handbook of the Physics and Chemistry of Rare Earths* vol 17, ed K A Gschneidner Jr and L Eyring (Amsterdam: North-Holland) ch 114
[2] Lebech B, Fischer P and Rainford B D 1971 *Rare Earths and Actinides (Inst. Phys. Conf. Digest 3) (Durham)* (Bristol: Institute of Physics Publishing) p 43
[3] Rossat-Mignod J, Burlet P, Villain J, Bartholin H, Wang Tcheng-Si and Florence D 1977 *Phys. Rev.* B **16** 440
[4] Fischer P, Lebech B, Meier G, Rainford B D and Vogt O 1978 *J. Phys. C: Solid State Phys.* **11** 345
[5] Meier G, Fischer P, Hälg W, Lebech B, Rainford B D and Vogt O 1978 *J. Phys. C: Solid State Phys.* **11** 1173
[6] McWhan D B, Vettier C, Isaacs E D, Ice G E, Siddons D P, Hastings J B, Peters C and Vogt O 1990 *Phys. Rev.* B **42** 6007
[7] Langridge S, Stirling W G, Lander G H and Rebizant J 1994 *Phys. Rev.* B **49** 12 010
[8] Langridge S, Stirling W G, Lander G H and Rebizant J 1994 *Phys. Rev.* B **49** 12 022
[9] Paixão J A, Lander G H, Tang C C, Stirling W G, Blaise A, Burlet P, Brown P J and Vogt O 1993 *Phys. Rev.* B **47** 8634
[10] Watson D, Forgan E M, Nuttall W J, Stirling W G and Fort D 1996 *Phys. Rev.* B **53** 726
[11] Rossat-Mignod J, Burlet P, Quezel S, Effantin J M, Delaĉote D, Bartholin H, Vogt O and Ravot D 1983 *J. Magn. Magn. Mater.* **31–34** 398
[12] Rossat-Mignod J, Effantin J M, Burlet P, Chattopadhyay T, Regnault L P, Bartholin H, Vettier C, Vogt O, Ravot D and Achart J C 1985 *J. Magn. Magn. Mater.* **52** 111
[13] Lebech B, Broholm C, Clausen K and Vogt O 1986 *J. Magn. Magn. Mater.* **52** 111
[14] Rainford B, Tuberfield K C, Busch G and Vogt O 1968 *J. Phys. C: Solid State Phys.* **1** 679
[15] Lebech B and Hae Seop Shim 1996 private communication

[16] Kasuya T, Kwon Y S, Suzuki T, Nakanishi K, Ishiyama F and Takegahara K 1990 *J. Magn. Magn. Mater.* **90+91** 389
[17] Kioussis N, Cooper B R, Willis J M and Sheng Q G 1990 *Physica* B **163** 107
[18] Siemann R and Cooper B R 1980 *Phys. Rev. Lett.* **44** 1015
[19] Kasuya T 1995 *Physica* B **215** 88
[20] Kasuya T, Sakai O, Tanaka J, Kitazawa H and Suzuki T 1987 *J. Magn. Magn. Mater.* **63+64** 9
[21] Hulliger F, Landolt M, Ott H R and Schmelczer R 1975 *J. Low Temp. Phys.* **20** 269
[22] Moncton D E, Gibbs D and Bohr J 1986 *Nucl. Instrum. Methods* A **246** 839
[23] Vogt O, unpublished
[24] Blume M and Gibbs D 1988 *Phys. Rev.* B **37** 1779
[25] Hill J P and McMorrow D F 1996 *Acta Crystallogr.* A **52** 236
[26] Gibbs D, Harshman D R, Isaacs E D, McWhan D B, Mills D and Vettier C 1988 *Phys. Rev. Lett.* **61** 1241
[27] Hannon J P, Trammell G T, Blume M and Gibbs D 1988 *Phys. Rev. Lett.* **61** 1245
[28] Hill J P, Helgesen G and Gibbs D 1995 *Phys. Rev.* B **51** 10 336
[29] Blume M 1988 *J. Appl. Phys.* **57** 3615
[30] Tsunoda Y, Mori M, Kunitomi N, Teraoka Y and Kanamori J 1974 *Solid State Commun.* **14** 287
[31] Gibbs D, Moncton D E, D'Amico K L, Bohr J and Grier B H 1985 *Phys. Rev. Lett.* **55** 234
[32] Cowley R A and Bates S 1988 *J. Phys. C: Solid State Phys.* **21** 4113
[33] Vigliante A, Hill J P, McMorrow D F, Helgesen G, Gibbs D, Ward R C C and Wells M R 1997 unpublished
[34] Lander G H, Bohr J and Gibbs D 1989 *Brookhaven National Laboratory NSLS Annual Report* BNL52218
[35] Hamrick M D 1994 *PhD Thesis* Rice University, TX